



Article

3D Printing Technique for Experimental Modeling of Hydraulic Structures: Exemplary Scaled Weir Models

Mario Oertel *  and Xiaoyang Shen 

Hydraulic Engineering Section, Faculty of Mechanical and Civil Engineering, Helmut-Schmidt-University Hamburg, University of the Federal Armed Forces, 22043 Hamburg, Germany; xiaoyang.shen@hsu-hh.de

* Correspondence: mario.oertel@hsu-hh.de

Abstract: 3D printing is a fast growing industry and is affecting many areas of our daily lives, e.g., in medical fields, mechanics, as well as engineering. For hydraulic experimental modeling, this technique offers a new alternative that could enable a more sufficient and rapid model fabrication, especially for models that feature complex geometries. The present study thus evaluates the feasibility of applying 3D printing to fabricate scaled hydraulic experimental models for laboratory use. Various weir models were printed and compared to conventionally produced reference models in terms of the fabrication process, resulting discharge coefficients, and hydraulic performance. Results show that while being more cost- and time-effective during the fabrication process, properly 3D printed models were able to fulfill experimental requirements and deliver accurate results with a relative deviation less than 5% compared to conventionally fabricated models. The printing layer height was found to be the most critical parameter influencing the model's final quality. Associated with the additive building approach, surface irregularities of 3D printed models were noted to be able to cause undesired nappe behavior, which might affect experimental results under certain conditions. To avoid such issues, a reduction of plotted layer heights or additional surface improvements could be helpful. Based on experimental results and visual assessments, 0.4 mm layer height can be recommended as a good compromise for model configurations tested herein.

Keywords: piano key weir; discharge coefficient; 3D printing; hydraulic model fabrication; hydraulic experiments



Citation: Oertel, M.; Shen, X. 3D Printing Technique for Experimental Modeling of Hydraulic Structures: Exemplary Scaled Weir Models. *Water* **2022**, *14*, 2153. <https://doi.org/10.3390/w14142153>

Academic Editor:
Francesco Gallerano

Received: 25 May 2022

Accepted: 4 July 2022

Published: 6 July 2022

Publisher's Note: MDPI stays neutral with regard to jurisdictional claims in published maps and institutional affiliations.



Copyright: © 2022 by the authors. Licensee MDPI, Basel, Switzerland. This article is an open access article distributed under the terms and conditions of the Creative Commons Attribution (CC BY) license (<https://creativecommons.org/licenses/by/4.0/>).

1. Introduction

Experimental modeling has always been an important method in hydraulic structure research to replicate complex hydrodynamic phenomena that cannot be adequately simulated or calculated [1–3]. However, this often faces financial and technical challenges regarding the fabrication process, especially for complicated geometries. As an example, Figure 1 shows the geometry of a piano key weir, which is a special type of a non-linear weir that has been increasingly constructed in the last two decades [4]. Relative to regular linear weirs, its folded plan form and inclined overhangs enable an increased discharge capacity as well as an optimized footprint. Due to the complex geometry, the fabrication process is complicated and thus time- and cost-consuming. Although numerical simulations are nowadays widely used, they still need to be validated and calibrated via experimental or in situ data. Especially for highly turbulent and aerated flows, numerical model results could include undesired uncertainties and may require extensive computation time. Hence, improving the experimental model's fabrication process is of major importance for effective research campaigns in hydraulics laboratories.

3D printing, formally called additive manufacturing, describes the transformative approach that rapidly creates layer-based physical objects from digital model data [5]. Since the invention of Stereolithography (STL) by Charles Hull in 1985 [6], 3D-printing technology has gone through decades of development and offers novel possibilities for

model prototyping, which has been applied in many areas of our daily lives; e.g., in medical fields, mechanics, and engineering. As examples: 3D printed implants in customized sizes have been developed to improve surgical outcome in medical applications; the Volkswagen group uses 3D printing to produce auxiliary tools [7]; in 2021 the first 3D printed residential building was constructed in Germany by the company PERI. Relative to mass-production, 3D printing techniques allow constant production costs independently from quantity aspects, which is a huge advantage especially for scientific research fields where normally only a small amount of model prototypes is needed. Commercially, enormous production can also be achieved according to Replication Rapid-prototyper (RepRap) method [8], which is basically a quasi self-producing process invented by Adrian Bowyer in 2004, e.g., [9]. The idea was to use 3D printers to print up to 70% of its own components. The 3D printer manufacturer company Prusa, for example, strictly follows this RepRap technology. Among the several different types of this kind of manufacture technology, stereolithography (SLA), selective laser sintering (SLS), and fused deposition modeling (FDM) are the most established methods, according to [5]. FDM, also known as Fused Filament Fabrication (FFF), is ideal for cost-effective, practical applications (e.g., experimental model fabrication in hydraulics laboratories). In contrast, SLA and SLS processes are characterized by higher resolution and accuracy. For FDM printers, various materials can be used: for instance, polylactic acid (PLA) is the most commonly used printing material due to a lower melting point and easier processability. However, it should be noted that PLA is not UV resistant and has a relatively low force resistance. Other available materials like acrylonitrile butadiene styrene (ABS) offer better resistance against sunlight, temperature, and external forces, but come with much higher printing condition requirements. Using the FDM method, filament material will be heated up to melting point and be turned into liquid state to create objects built by multiple layers. With this method, 3D printing enables a time- and cost-effective way to fabricate accurate experimental model configurations. Within the past few years, a few studies have successfully employed 3D printing for open-channel hydraulic researches: Ref. [10] utilized 3D printing technique to replicate gravel river beds together with digital elevation models obtained from stereo photogrammetry and reported that this fabrication method is suitable for obtaining realistic ground truth for known surfaces. However, the hydraulic properties of the printed river bed were not addressed. More recently, a similar approach was also adopted in Ref. [11] to build a 1:10 Froude-scaled laboratory bedrock-alluvial model, which has been tested under different discharge conditions. With the focus on the river bed topography and the correlating local hydraulics, the fabrication process and the relationship between printing quality and resulting flow characteristics were not analyzed in detail. Up to date, very limited information can be found regarding the application of this new model fabrication process in hydraulic structure studies. Especially for supercritical and boundary layer flows, the printing quality might be a critical factor affecting the resulting hydraulic characteristics. In addition, it is still unclear whether a 3D printed model would be able to fulfill the experimental requirements and if it can represent identical hydrodynamic characteristics as conventionally fabricated models. This study thus aims to address the workflow of the model fabrication via 3D printing and evaluate exemplary applications in experimental modeling of hydraulic structures.

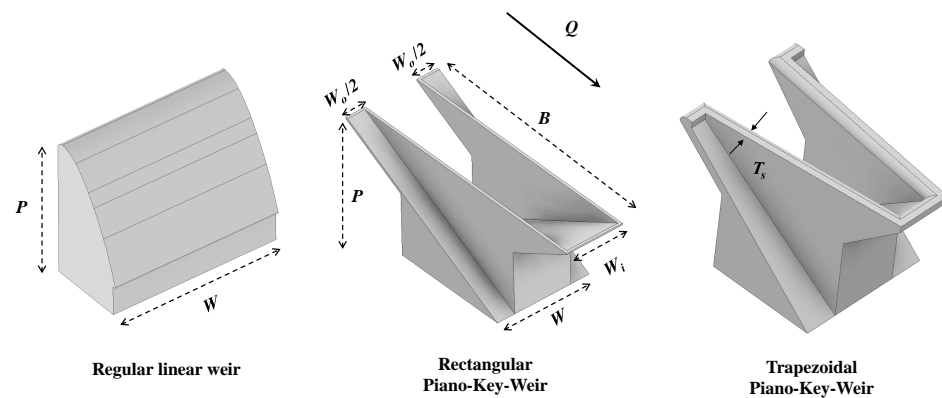


Figure 1. Tested weir configurations, **left:** regular linear weir, **middle:** rectangular piano key weir, **right:** trapezoidal piano key weir.

2. Experimental Setup and Methods

Three different weir configurations were included within the present study to systematically investigate whether a 3D printed model would be able to represent identical hydraulic properties as conventionally fabricated models and to check printed models for possible scale effect influences. Various print-settings have been applied and compared to evaluate the most important plotting parameters for accurate results. The first investigated model is a regular linear weir fabricated by the company Armfield with Glas Reinforced Polyester (GRP) (Figures 1 left and 2 left). This weir was duplicated via 3D printing technique with three different plotting properties: (a1) 0.2 mm layer height with horizontal orientation, (b1) 0.4 mm layer height with horizontal orientation, and (c1) 0.4 mm layer height with vertical orientation. In order to further compare the fabrication time and costs of more complex configurations, a single-cycle rectangular piano key weir was fabricated via (a2) conventional method using glued Acrylic glass and (b2) 3D printing technique using PLA material respectively (Figures 1 middle and 2 middle) and tested under equivalent hydraulic conditions. Furthermore, a third model configuration was used to test the potential layer height influence on different sized trapezoidal piano key weirs: (a3) $p = 30$ cm, and (b3) $p = 40$ cm (Figures 1 right and 2 right). Both models were printed with horizontal layer orientation and corresponding layer heights of 0.4 mm and 0.6 mm, respectively. The main geometric parameters and utilized materials of all tested models are summarized in Table 1.

As mentioned in various studies [12,13] the surface roughness and friction factor of 3D prints highly depend on the print-settings (e.g., layer height, layer orientation, print-speed, etc.) as well as the model complexity. Based on experimental results, Ref. [14] proposed an analytical equation for the first-order estimation of the final surface roughness of 3D printed models in dependence of various printing parameters. With the help of this equation, the estimated maximal surface roughness for the current tested models were $15.8\ \mu\text{m}$, $22.7\ \mu\text{m}$, and $36.9\ \mu\text{m}$ for models printed with 0.2 mm, 0.4 mm, and 0.6 mm layer heights, respectively.



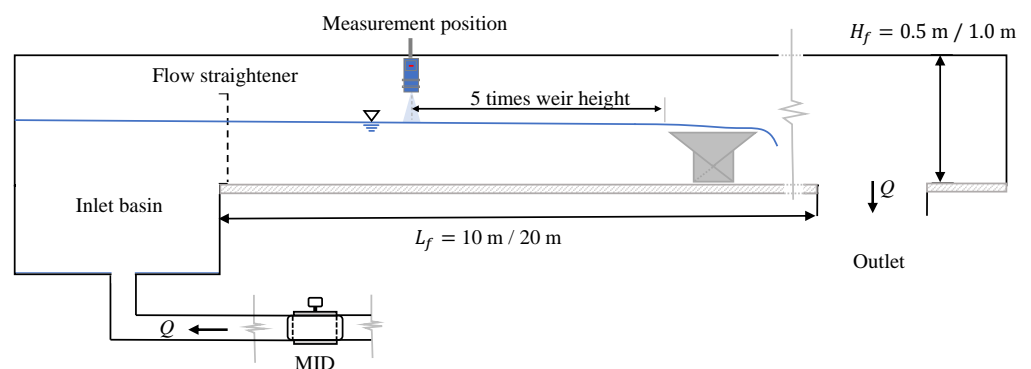
Figure 2. Investigated weir geometries, **left:** regular linear weirs, **middle:** rectangular piano key weirs, **right:** trapezoidal piano key weirs.

Table 1. Summary of model specifications.

Model	Layer Orientation	Material	Layer Height (mm)	P (mm)	L^* (mm)	B (mm)	W (mm)	W_i/W_o (mm)
Regular Weir models (RW)								
RW _{Armfield}	-	GRP **	-	239	300	133	300	-
RW _{0.2-h}	horizontal	PLA	0.2	239	300	133	300	-
RW _{0.4-h}	horizontal	PLA	0.4	239	300	133	300	-
RW _{0.4-v}	vertical	PLA	0.4	239	300	133	300	-
Rectangular Piano Key Weir models (RPKW)								
RPKW _{acrylic}	-	Acrylic glass	-	315	1858	789	300	1.5
RPKW _{0.4-h}	horizontal	PLA	0.4	315	1858	789	300	1.5
Trapezoidal Piano Key Weir models (TPKW)								
TPKW _{P30}	horizontal	PLA	0.4	300	1103	480	300	1.0
TPKW _{P40}	horizontal	PLA	0.6	400	1356	640	1000	1.0

Notes: * L represents the total centerline crest length of the weir; ** Glas Reinforced Polyester.

Models with 300 mm width were fabricated using a Creality CR-10 Max 3D-printer, which offers a printing domain up to $L_{pd} \times B_{pd} \times H_{pd} = 450 \text{ mm} \times 450 \text{ mm} \times 470 \text{ mm}$. A large-scaled trapezoidal piano key weir model with 1 m total width (TPKW_{P40}) was printed with a Bigrep One.4 with a maximum plotting volume of $L_{pd} \times B_{pd} \times H_{pd} = 1005 \text{ mm} \times 1005 \text{ mm} \times 1005 \text{ mm}$. Due to different model sizes, measurement campaigns were carried out in two rectangular horizontal glass flumes (flume 1 is $W_f = 0.3 \text{ m}$ wide, $H_f = 0.5 \text{ m}$ deep and $L_f = 10 \text{ m}$ long; flume 2 is $W_f = 1.0 \text{ m}$ wide, $H_f = 1.0 \text{ m}$ deep and $L_f = 20 \text{ m}$ long). Flow straighteners were installed at the flow entrance of both flumes to ensure a uniform approaching flow. All models were tested under equivalent hydraulic conditions and data were collected under steady-state condition. Discharges were measured via magnetic inductive flow-meters (Fabricate: Krohne, Optiflux 2000, accuracy $\pm 0.3\%$); flow depths were determined via point gauge (accuracy $\pm 0.1 \text{ mm}$) and multiple ultrasonic sensors (Fabricate: Microsonic, resolution: 0.025 mm , accuracy $\pm 1\%$). The schematic experimental set-up is illustrated in Figure 3.

**Figure 3.** Schematic experimental set-up for both flumes.

3. Comparison between 3D Printing and Conventional Fabrication Process

Similar to other fabrication methods, 3D printing starts with detailed model sketching. As a first step, a digital 3D model needs to be prepared and exported into a common 3D file format (e.g., STL). This specific file will be transformed by a slicing software (e.g., Cura, Slic3r, Prusa Slicer etc.) into a G-code, which includes all desired digital printing instructions for the specific 3D printer. The final model surface quality mainly depends on

the layer height and printing speed while the infill density as well as the wall thickness are crucial parameters for the model stability. Nonetheless, additional parameter settings—like layer orientation, support structures, and print bed leveling – are relevant for quality aspects. The general printing process starts with pre-heating the printing bed and the extruder. Subsequently, the extruder will transform the filament into a viscous mass, which could be pressed through the nozzle and lubricated on the print bed or on existing layers, where a massive temperature drop turns it back into solid state. It should be noted that different 3D printers are built with various printing mechanisms. A Bigrep One, for example, comes with a fixed printing bed with movable nozzles in all three space directions while for a Creality CR-10 max the printing bed moves along the y -direction. By adding layer on layer, the final 3D geometry will be created in a vertical direction. Figure 4 illustrates an exemplary procedure from digital data to the final print.



Figure 4. From digital data to final model, **left:** STL model, **middle:** sliced layer model, **right:** final print.

Contrary to the almost fully automated 3D printing process, the conventional model fabrication can differ majorly depending on the model material. Among various materials, transparent acrylic glass is often preferred in hydraulics laboratories. Focusing on the investigated rectangular PKW as an example (Figure 2 middle), the final model was made of various components. In order to obtain the precise geometry, each component needs to be carefully measured, laser-cut, and finally assembled using special glue. This kind of conventional fabrication process is generally complicated and time-consuming, especially for complex geometries like piano key weirs. Moreover, unlike mass-production in industry, only a small amount of fabricated models will normally be needed for research purpose within a hydraulics laboratory. The prefabrication of unique model parts usually correlates to longer delivery times and higher unit prices. As a consequence, the acrylic glass PKW model tested within the present study comes with material costs of more than EUR 300 and require a delivery time of approximately 1 week since it consists of various highly customized parts; another 8–12 hours were needed to manually build the PKW geometry and wait for the glue to reach the optimum bonding status. In addition, the accuracy of the final model geometry highly depends on human assembly skills, which cannot be standardized. For comparative studies, in which a series of geometrically similar models is needed, manual assembling could cause significant potential uncertainties regarding the accuracy of the model geometry and final results.

Table 2 presents a detailed comparison of material costs and fabrication times for all investigated model geometries. Since the 3D designing process can be considered as equivalent for all fabricated models it is not included in the calculation of fabrication time. Generally, 3D printing offers a good alternative with reduced fabrication time, cost, as well as human resource while the printing time and material consumption are largely dependent on the model geometry, model size, infill density, and printing layer height.

Table 2. Comparison of material costs and fabrication times.

Model	Material	Layer Height	Infill Density	Model Weight	Cost (Euro)	Time (Hours)
Regular linear weir models (RW)						
RW _{0.2-h}	PLA	0.2 mm	15%	1.6 kg	~40	120
RW _{0.4-h}	PLA	0.4 mm	15%	1.8 kg	~45	42
RW _{0.4-v}	PLA	0.4 mm	15%	1.8 kg	~45	40
Rectangular Piano Key Weir models (RPKW)						
RPKW _{acrylic}	acrylic glass	-	-	8 kg	~300	180
RPKW _{0.4-h}	PLA	0.4 mm	15%	4.6 kg	~115	96
Trapezoidal Piano Key Weir models (TPKW)						
TPKW _{P30}	PLA	0.4 mm	15%	2 kg	~50	50
TPKW _{P40}	PLA	0.6 mm	15%	24 kg	~750	192

Next to an effective fabrication process, 3D printing can also have advantages concerning environmental aspects compared with classical fabrication methods. PLA, for example, represents a natural product that is made of corn meal; thus it is bio-degradable (it should be noted that ABS and PETG are highly synthetic). Misprints and old models can thus be re-used within a recycling process, where old 3D prints will be shredded, heated, and reformed to new filament. For the future it can be expected that such recycling machines will be commercially available on the market, which would be a huge step towards a sustainable 3D printing application.

The relatively imperfect surface finish could be mentioned as a disadvantage, especially for model parts with curved surfaces due to the layer-by-layer printing approach. These surface irregularities increase with increasing layer heights. Additionally, due to the specific material properties of PLA, the printed model is usually non-transparent and not UV-resistant. Hence, 3D printings made of PLA are easy-to-use but not suitable for permanent structures; e.g., for outdoor investigations. Overall, the advantages and disadvantages of 3D printing relative to conventional fabrication methods using acrylic glass are summarized in Table 3.

Table 3. Advantages and disadvantages of 3D printing relative to conventional fabrication methods.

Advantages	Disadvantages
<ul style="list-style-type: none"> • automated printing process with reduced human input • high precision model fabrication • rapid prototyping for models with complex geometries • standardized model quality • low incremental cost of variety • recyclable material usage 	<ul style="list-style-type: none"> • imperfect surface finish • durability • insufficient UV-resistance (PLA)

4. Exemplary Experimental Results

Specifically for hydraulic structure researches, physical weir models are widely used with the purpose to predict the discharge capacity of prototypes or configurations with adjusted geometries. The dimensionless discharge coefficient C_{dL} is accepted as a standard parameter to represent the discharge capacity of weir structures and can be calculated using the classical weir flow formula, e.g., [15,16]:

$$Q = \frac{2}{3} \cdot C_{dL} \cdot L \cdot \sqrt{2g} \cdot H_T^{3/2} \quad (1)$$

where: Q = discharge; C_{dL} = discharge coefficient related to total crest length (represents the discharge capacity per unit weir length); g = acceleration due to gravity; H_T = total upstream head = piezometric head (h_T) measured relative to the weir crest plus velocity head ($H_T = h_T + \bar{v}^2(2g)^{-1}$), \bar{v} = mean depth-averaged velocity upstream the weir.

Based on the experimental data, the head-discharge relationship as well as the resulting C_{dL} -values for 3D prints and conventionally fabricated models were compared in Figures 5 and 6. The parameter h_T in Figure 5 top denotes the overfall height and Δh_T [bottom] indicates the absolute difference of overfall heights between 3D printed models compared with the corresponding conventionally fabricated reference model.

It can be clearly seen that for both weir geometries (RW and RPKW), 3D printed models can almost perfectly reproduce the same hydraulic performance of models that were built via conventional methods. Absolute differences of measured flow depths were within 1.5 mm (Figure 5 bottom) and the resulting C_{dL} values were also reproduced adequately (Figure 6). According to Figure 7, the relative errors of C_{dL} -values between 3D printed and conventionally fabricated models were less than 5% for all performed discharges.

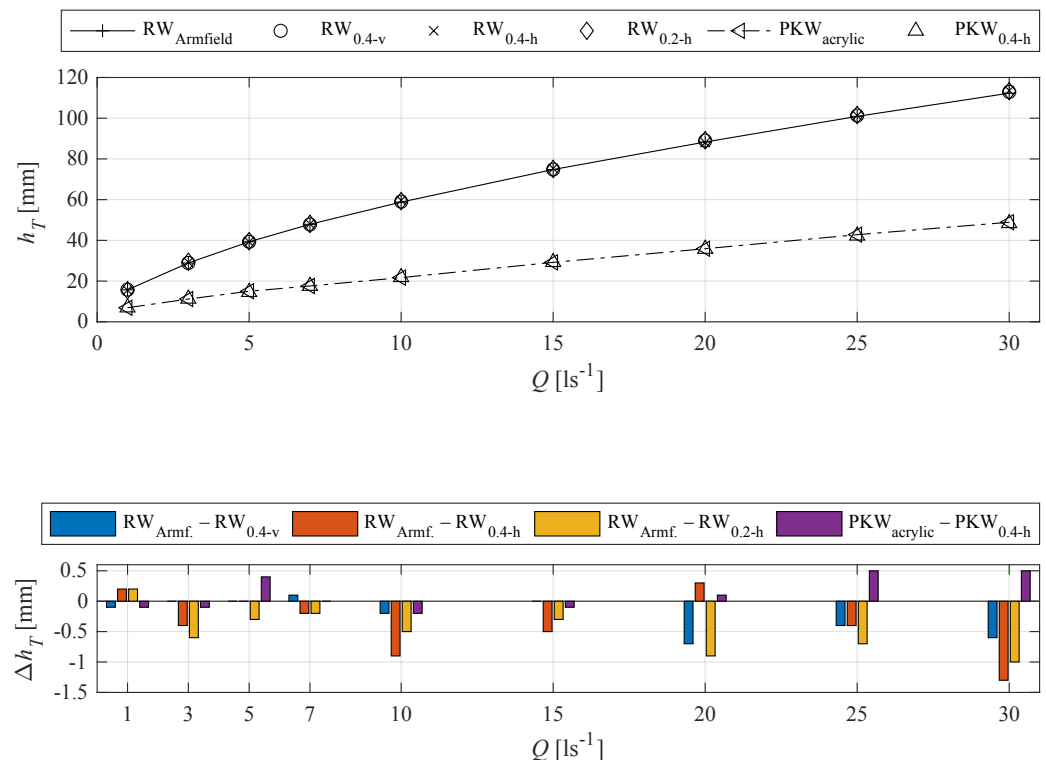


Figure 5. Rating curves for all investigated model runs (top) and absolute measurement differences (bottom).

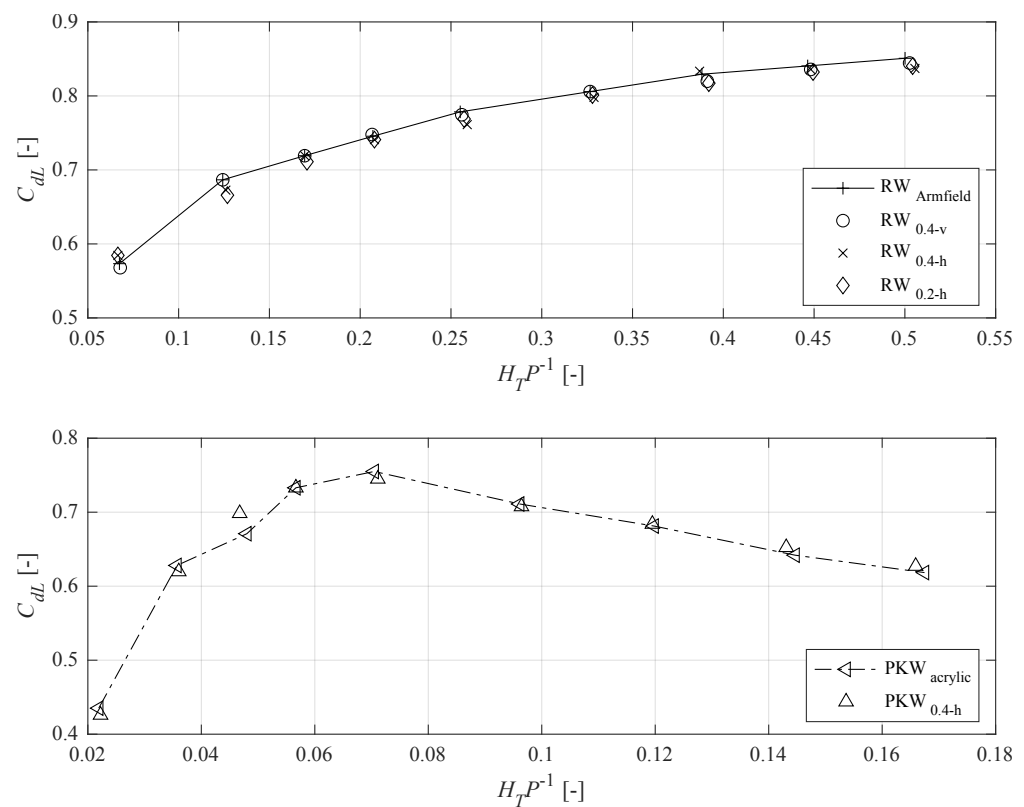


Figure 6. Discharge coefficients C_{dL} , **top:** regular weirs, **bottom:** piano key weirs.

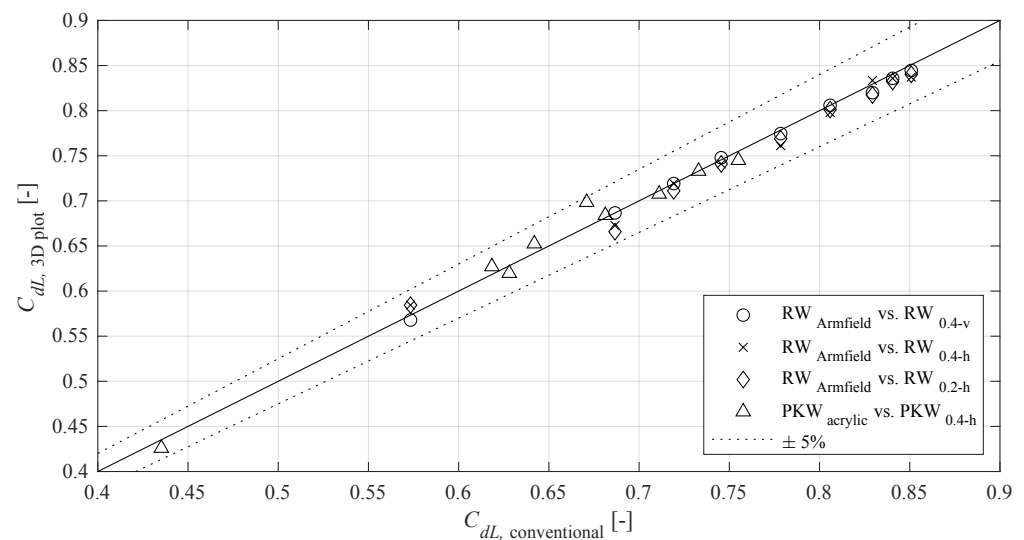


Figure 7. Discharge coefficients C_{dL} comparison, conventional fabrication methods vs. 3D plot.

Overall, the results indicate that printing layer heights up to 0.4 mm and layer orientation showed negligible influence on the hydraulic performance of tested model configurations. However, as mentioned in the previous section, surface irregularities of 3D printed models intensify with increasing layer height and are more significant for curved surfaces. Two trapezoidal piano key weir (TPKW) configurations were thus additionally printed with quarter-round crest and greater layer height to further examine potential nappe effects that could be induced by surface irregularities. Similar as RPKW models, the smaller TPKW model is also single-cycled with 30 cm weir height and printed with 0.4 mm layer height. Nonetheless, it has a greater wall thickness in order to emphasize the surface irregularities on curved crests. Another upscaled model is 40 cm in height, and consists of

2.5 cycles with a total width of 100 cm. The model was printed with 0.6 mm layer height. According to Ref. [17], the cycle number does not affect the hydraulic behavior of a PKW due to its symmetrical geometry. Both TPKW models were tested with relative upstream heads $0.05 < H_T P^{-1} < 0.6$. As presented in Figure 8, significant nappe separation can be observed at the downstream crest apex for the upscaled model with 0.6 mm layer height for $H_T P^{-1} > 0.34$. A detailed observation of the nappe detachment is shown in Figure 9. Note that only one cycle of the upscaled model (TPKW_{P40}) is presented for a better comparison. Observations indicate that for high discharges, the surface roughness (above a certain level) will result in deviated flow trajectory. However, for resulting discharge coefficients no appreciable differences between both tested configurations can be identified, as illustrated in Figure 10. It can be expected that these unevenly distributed air cavities could slightly elevate the overfall height and consequently affect the total efficiency if the upstream head further increases. A similar phenomenon was not observed for the smaller scaled model (TPKW_{P30}) with 0.4 mm layer height.

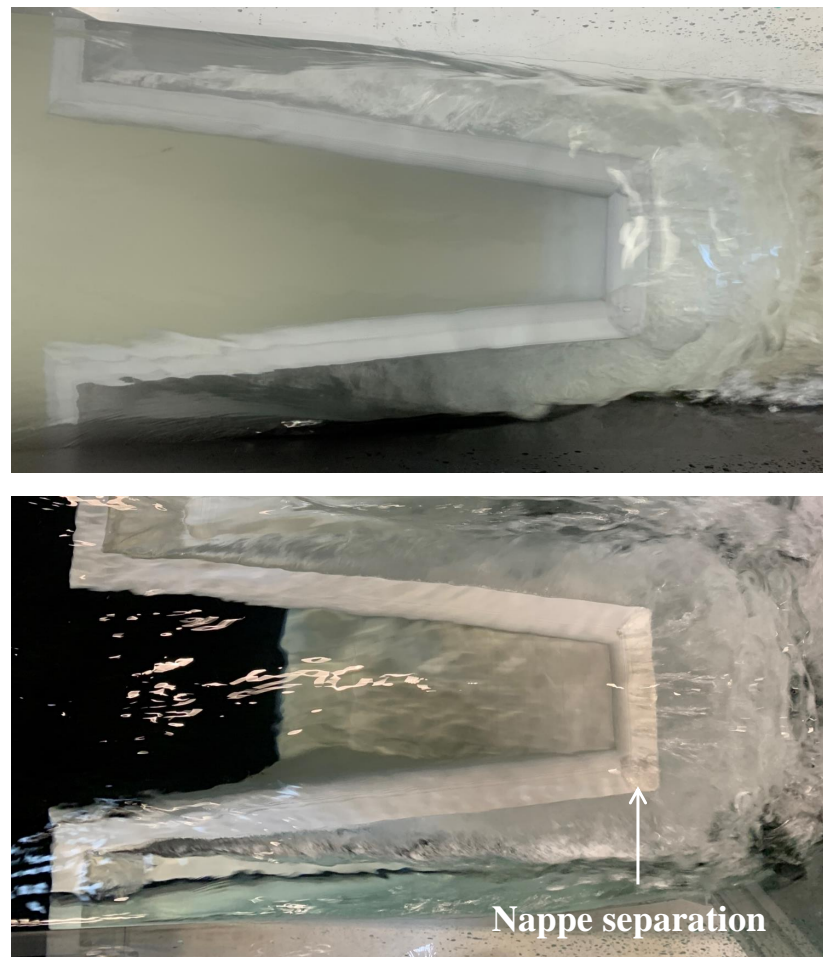


Figure 8. Comparison of nappe trajectory for trapezoidal piano key weir model at $H_T P^{-1} = 0.34$, **top:** TPKW_{P30}, **bottom:** TPKW_{P40}.



Figure 9. Detail of nappe separation induced by surface roughness, TPKW_{P40}, **left:** top view, **right:** side view, flow direction from left to right.

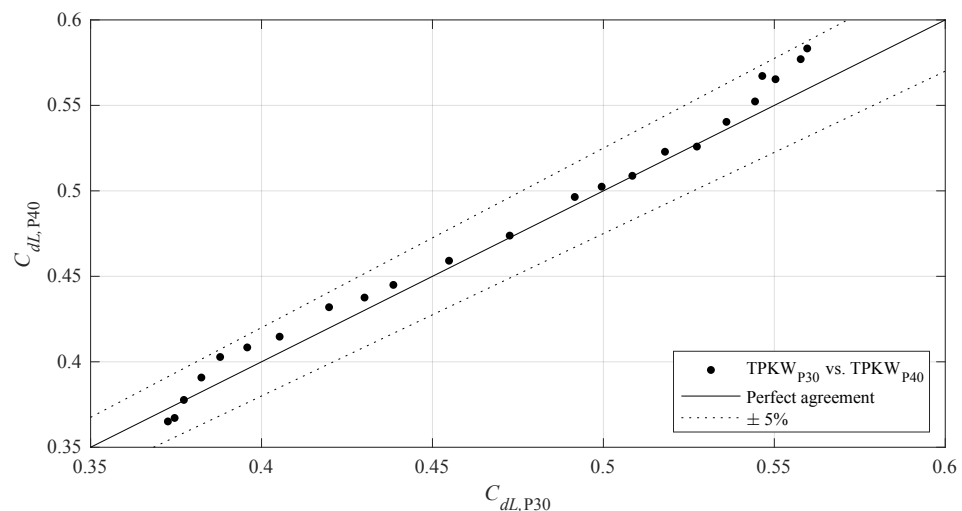


Figure 10. Comparison between TPKW_{P30} and TPKW_{P40} for the resulting C_{dL} -values.

In summary, the experimental results and laboratory observations indicate that properly printed models are able to fulfill general experimental requirements and represent similar hydrodynamic performance as conventionally fabricated models. It should be noted that the imperfect surface finish of 3D printed models could lead to unstable nappe behavior (boundary layer influences), which may affect experimental results under certain conditions.; e.g. also concerning scale effects [18,19]. Such situations could be improved or avoided by using finer layer heights or adjusting the surface texture to an appropriate orientation. Based on the experiments conducted within the present study, 0.4 mm layer can be recommended as a good compromise for similar model configurations and sizes. Further layer refinements seem to be unnecessary since no major improvement in experimental results was achieved. Note that these findings might only relate to models with similar sizes or geometries as considered herein.

5. Conclusions

With recyclable material and reduced time, cost as well as human efforts in model fabrication processes, it can be expected that 3D printing techniques will be increasingly applied in hydraulics laboratories in the future. The present study examined various 3D printed configurations and compared them with conventionally fabricated reference models. Results indicate that appropriately printed models are able to not only fulfill

hydraulic experimental requirements but also represent identical hydraulic performance as conventional fabricated models. Nonetheless, although negligible differences were measured in terms of resulting discharge coefficients, it was noted that the imperfect surface finish inherent with the additive building process could cause a deviated nappe behavior, which might affect the final experimental results under certain conditions. To prevent such issues, reduced printing layer heights or additional model surface improvements are necessary. For the specific model sizes and geometries tested herein, 0.4 mm layers can be recommended to be sufficient since no further improvements were achieved with refined layer heights.

Note that the results of this study are limited to the tested weir geometries and configurations printed with PLA material. Beyond weir structures, further studies are recommended to also include other experimental models and filament materials as well as friction factor analysis.

Author Contributions: Conceptualization, M.O.; methodology, M.O. and X.S.; software, M.O. and X.S.; validation, M.O. and X.S.; data curation, M.O. and X.S.; writing—original draft preparation, M.O. and X.S.; writing—review and editing, M.O. and X.S.; visualization, M.O. and X.S.; supervision, M.O.; project administration, M.O.; funding acquisition, M.O. All authors have read and agreed to the published version of the manuscript.

Funding: This research received no external funding.

Conflicts of Interest: The authors declare no conflict of interest.

Notations

The following notations are used in this manuscript:

B	model length (m)
C_{dL}	discharge coefficient related to total crest length (m)
g	gravity acceleration (m s^{-2})
H	model height (m)
H_f	flume depth (m)
H_{pd}	3D plotter printing domain (m)
H_t	upstream total head (m)
L	total crest length of tested weirs (m)
L_f	flume length (m)
L_{pd}	3D plotter printing domain (m)
P	weir height (m)
Q	discharge (l s^{-1})
RW	regular linear weirs
$RW_{Armfield}$	reference regular linear weir model fabricated by the company Armfield
$RW_{0.2-h}$	regular linear weirs 3D printed with horizontal layers and 0.2 mm layer height
$RW_{0.4-h}$	regular linear weirs 3D printed with horizontal layers and 0.4 mm layer height
$RW_{0.4-v}$	regular linear weirs 3D printed with vertical layers and 0.4 mm layer height
$RPKW$	piano key weir with rectangular plan form geometry
$RPKW_{acrylic}$	reference piano key weir model fabricated conventionally with acrylic glass
$RPKW_{0.4-h}$	piano key weir model 3D printed with horizontal layers and 0.4 mm layer height
$TPKW$	piano key weir with trapezoidal plan form geometry
$TPKW_{P30}$	3D printed trapezoidal piano key weir with 30 cm weir height
$TPKW_{P40}$	3D printed trapezoidal piano key weir with 40 cm weir height
W	model width (m)
W_f	flume width (m)
W_i	piano key weir inlet key width (m)
W_o	piano key weir outlet key width (m)
W_{pd}	3D plotter printing domain (m)

References

1. Bung, D.B. Laboratory Models of Free-Surface Flows. In *Rivers—Physical, Fluvial and Environmental Processes*; GeoPlanet: Earth and Planetary Sciences; Rowiński, P., Radecki-Pawlik, A., Eds.; Springer: Cham, Switzerland; Heidelberg, Germany; New York, NY, USA; Dordrecht, The Netherlands; London, UK, 2015; ISBN 978-3-319-17718-2. <https://doi.org/10.1007/978-3-319-17719-9>.
2. Erpicum, S.; Crookston, B.M.; Bombardelli, F.; Bung, D.B.; Felder, S.; Mulligan, S.; Oertel, M.; Palermo, M. Hydraulic structures engineering: An evolving science in a changing world. *WIREs Water* **2019**, *8*, e1505. <https://doi.org/10.1002/wat2.1505>.
3. USBR. *Hydraulic Laboratory Techniques, A Guide for Applying Engineering Knowledge to Hydraulic Studies Based on 50 Years of Research and Testing Experience*; United States Bureau of Reclamation (USBR), Department of the Interior, Water and Power Resources Service: Denver, CO, USA, 1980.
4. Crookston, B.M.; Erpicum, S.; Tullis, B.P.; Laugier, F. Hydraulics of Labyrinth and Piano Key Weirs: 100 Years of Prototype Structures, Advancements, and Future Research Needs. *ASCE J. Hydraul. Eng.* **2019**, *145*, 02519004.
5. Gibson, I.; Rosen, D.; Stucker, B. *Additive Manufacturing Technologies: 3D Printing, Rapid Prototyping, and Direct Digital Manufacturing*, 2nd ed.; Springer: New York, NY, USA, 2015; ISBN 978-1-4939-2112-6.
6. Jacobs, P. Rapid prototyping and manufacturing: Fundamentals of stereolithography. In *Society of Manufacturing Engineers*, 1st ed.; Society of Manufacturing Engineers: Dearborn, MI, USA, 1992; ISBN 0-87263-425-6.
7. Rülke, C.M. Audi Expands Polymer 3D Printing in Production. Audi Mediacenter. 2019. Available online: <https://www.audi-mediacycenter.com/en/press-releases/audi-expands-polymer-3d-printing-in-production-11466> (accessed on 24 August 2021).
8. Jones, R.; Haufe, P.; Sells, E.; Iravani, P.; Olliver, V.; Palmer, C.; Bowyer, A. *RepRap—The Replicating Rapid Prototyper, Robotica*; Cambridge University Press: Cambridge, UK, 2011; Volume 29, pp. 177–191.
9. Bowyer, A. 3D printing and humanity's first imperfect replicator. *3D Print. Addit. Manuf.* **2014**, *1*, 4–5. <https://doi.org/10.1089/3dp.2013.0003>
10. Bertin, S.; Friedrich, H.; Delmas, P.; Chan, E.; Gimelfarb, G. DEM quality assessment with a 3D printed gravel bed applied to stereo photogrammetry. *Photogramm. Rec.* **2019**, *29*, 241–246.
11. Hodge, R.A.; Hoey, T.B. A Froude-scaled model of a bedrock-alluvial channel reach: 1. Hydraulics. *JGR Earth Surf.* **2016**, *121*, 1578–1596.
12. Mazen, A.; McClanahan, B.; Weaver, J.M. Factors affecting ultimate tensile strength and impact toughness of 3D printed parts using fractional factorial design. *Int. J. Adv. Manuf. Technol.* **2022**, *119*, 2639–2651. <https://doi.org/10.1007/s00170-021-08433-0>.
13. O'Brien, J.H.; Evers, J.; Tempelman, E. Surface roughness of 3D printed materials: Comparing physical model measurements and human perception. *Mater. Today Commun.* **2019**, *19*, 300–305.
14. Fuad, J.S. *Quantifying the Surface Roughness of a 3D Printed Model*; The University of New South Wales Canberra at the Australian Defence Force Academy: Campbell, ACT, Australia, 2019.
15. Oertel, M. Piano key weir research: State-of-the-art and future challenges. In *Proceedings of the 7th International Symposium on Hydraulic Structures*, Aachen, Germany, 15–18 May 2018; pp. 1–8.
16. Shen, X.; Oertel, M. Comparative study of nonsymmetrical trapezoidal and rectangular Piano Key Weirs with varying key width ratios. *ASCE J. Hydraul. Eng.* **2021**, *147*, 04021045. [https://doi.org/10.1061/\(ASCE\)HY.1943-7900.0001942](https://doi.org/10.1061/(ASCE)HY.1943-7900.0001942).
17. Pfister, M.; Boillat, J.L.; Schleiss, A.; Laugier, F.; Leite Ribeiro, M. Piano Key Weirs as efficient spillway structure. In *Proceedings of the 24th Congress of CIGB—ICOLD*, EPFL, Kyoto, Japan, 2–8 June 2012.
18. Oertel, M. Size-scale effects of an a-type piano key weir. In *Proceedings of the 38th IAHR World Congress—Water: Connecting the World*, Panama City, Panama, 1–6 September 2019; pp. 1930–1939.
19. Tullis, B.P.; Crookston, B.M.; Young, N. Scale effects in free-flow nonlinear weir head-discharge relationships. *ASCE J. Hydraul. Eng.* **2020**, *146*, 04019056.